

Article

# Experimental Study on the Mass Flow Rate of the Self-Pressurizing Propellants in the Rocket Injector

Tomasz Palacz \*  and Jacek Cieřlik

AGH University of Science and Technology, Al. Mickiewicza 30, 30-059 Cracow, Poland; cieslik@agh.edu.pl

\* Correspondence: palacz@agh.edu.pl

**Abstract:** High vapor pressure propellants such as nitrous oxide are widely used in experimental hybrid and liquid rockets as they can be used in a self-pressurization mode, eliminating the need for external pressurization or pumps and simplifying the design of the rocket system. This approach causes the two-phase flow in the feed system and the injector orifices, which cannot be easily modeled and accounted for in the design. A dedicated test stand has been developed to better understand how the two-phase flow of the self-pressurizing propellant impacts the mass flow characteristics, enabling the simulation of the operating conditions in the rocket engine. The injectors have been studied in the range of  $\Delta P$ . The flow regimes have been identified, which can be predicted by the SPI and HEM models. It has been shown that the two-phase flow quality upstream of the injector may impact the discharge coefficient in the SPI region and the accuracy of the HEM model. It has been found that the transition to the critical flow region depends on the L/D ratio of the injector orifice. A series of conclusions can be drawn from this work to design the rocket injector with a self-pressurizing propellant to better predict the mass flow rate and ensure stable combustion.

**Keywords:** nitrous oxide; mass flow rate; self-pressurization; injector; two-phase flow



**Citation:** Palacz, T.; Cieřlik, J. Experimental Study on the Mass Flow Rate of the Self-Pressurizing Propellants in the Rocket Injector. *Aerospace* **2021**, *8*, 317. <https://doi.org/10.3390/aerospace8110317>

Academic Editor: Carmine Carmicino

Received: 8 August 2021

Accepted: 25 October 2021

Published: 26 October 2021

**Publisher's Note:** MDPI stays neutral with regard to jurisdictional claims in published maps and institutional affiliations.



**Copyright:** © 2021 by the authors. Licensee MDPI, Basel, Switzerland. This article is an open access article distributed under the terms and conditions of the Creative Commons Attribution (CC BY) license (<https://creativecommons.org/licenses/by/4.0/>).

## 1. Introduction

In the past two decades, there has been growing interest in new propellants for rocket engines and space propulsion, mainly driven by the search for “green” alternatives [1], but also for educational and experimental purposes [2]. Nitrous oxide has gained high popularity, especially as an oxidizer for hybrid rockets [3], as well as is considered for space thrusters [4]. It is relatively safe, non-toxic, and storable at room temperature, therefore easy to handle. Its key advantage is its high vapor pressure, which allows for self-pressurization. It eliminates the need for external pressurization with the inert gas or the pumping system, which greatly reduces the complexity and cost of the rocket system.

However, when used in self-pressurization mode, the nitrous oxide boils when its static pressure drops below its saturation pressure. Due to the pressure drop in the feed system, a large amount of vapor is formed, and nitrous oxide flows in two phases in both the feed system and the injector.

As the injector has a major impact on the stability and performance of the liquid or hybrid rocket by controlling the mass flow rate and playing a crucial role in isolating the combustion chamber and the feed system, it must be designed carefully. Injector performance is often presented in the form of the mass flow rate of a given propellant versus the pressure drop  $\Delta P$  across the injector. Most commonly, to model the mass flow rate through the injector orifice, the SPI (Single-Phase Incompressible) model is used, defined as:

$$\dot{m}_{\text{SPI}} = C_d A \sqrt{2\rho\Delta P}, \quad (1)$$

where  $C_d$  is the discharge coefficient,  $A$  is the cross-sectional area of the orifice, and  $\rho$  is the density of the propellant.  $\Delta P$  is the pressure drop across the injector given by  $\Delta P = P_1 - P_2$ , where  $P_1$  is the pressure upstream of the injector and  $P_2$  is downstream or chamber pressure.

Usually, the discharge coefficient  $C_d$  includes all factors reducing the mass flow rate from the theoretical value:

$$C_d = \frac{\dot{m}_{\text{measured}}}{\dot{m}_{\text{theoretical}}}, \quad (2)$$

The SPI model is often wrongly used to predict the injector performance with nitrous oxide as a propellant. The two-phase flow must be accounted for to correctly estimate the mass flow rate of the nitrous oxide or other high vapor pressure propellant, especially when using self-pressurization. The amount of vapor formed when flowing from the tank through the feed system and the injector may significantly vary depending on the factors such as operating conditions, pressure drop, and system design. To describe the amount of vapor in the two-phase flow, the flow quality is defined as:

$$QF = \dot{m}_v / \dot{m}_t, \quad (3)$$

where  $\dot{m}_v$  is the vapor mass flow rate and  $\dot{m}_t$  is total mass flow rate. Experiments by Hesson and Peck have shown that for the two-phase mixtures (in this case, the carbon dioxide), the QF has a considerable impact on the mass flow rate through the orifice [5]. Additionally, the flashing vapor in the injector, where the pressure drop is the highest, will “choke” the orifice limiting the mass flow rate. This phenomenon, called the critical flow, was also shown by Hesson and Peck on carbon dioxide. The critical flow is virtually independent of the downstream pressure.

The HEM (Homogeneous Equilibrium Model) model can be used to estimate the two-phase mass flow rate and predict the critical flow [6]. It assumes that the phases are in the thermodynamic equilibrium and there is no slip. It is given by:

$$\dot{m}_{\text{HEM}} = C_d A \rho_2 \sqrt{2(h_1 - h_2)}, \quad (4)$$

where  $\rho_2$  is the bulk density of the fluid in the downstream and  $h_1$  and  $h_2$  are enthalpies of the fluid upstream and downstream of the injector, respectively. It has been observed that the HEM model has reportedly underpredicted the mass flow rate for nitrous oxide by up to 20% [6–8]. Most of the researchers agree that it is due to the finite rate of the mass transfer between the liquid and vapor phases [9], although some have speculated that the HEM model’s inaccuracy for two-phase flow is related to the slip between the phases [10]. In fact, the typical rocket injector orifice rarely meets the thermodynamic equilibrium condition. The homogenous non-equilibrium model (HNE) accounts for the finite mass transfer rate by including a non-equilibrium multiplier that depends on the orifice length. It has been found that the HNE does not work well for the nitrous oxide and low length-to-diameter ratio ( $L/D$ ) of the orifices typically found in the rocket injector [6]. Dyer et al. proposed a model, which recognizes that the non-equilibrium effects are due to the superheating of the saturated liquid during compression and finite vapor bubble growth rate. Dyer model assumes that the predicted mass flow rate varies between the SPI and HEM models depending on the residence time [6]. For the infinitesimally small residence time, the flow would be purely liquid so that the SPI model would be correct. For the infinitesimally large residence time, the vapor would be formed, and the phases would reach thermal equilibrium so that the HEM model would be correct. The residence time is logically linked to the length-to-diameter  $L/D$  ratio of the injector orifice. Supposedly for larger  $L/D$ , the fluid has more time to reach thermal equilibrium, and the mass flow rate is closer to the value predicted by the HEM model. Using this model, the predicted mass flow rate values have been mostly within  $\pm 10\%$  of the measured mass flow rate [6]. The entropy-based engineering model for a self-pressurized saturated propellant feed system has been developed using the Dyer model to estimate the mass flow through the injector orifice. The experimental test results using nitrous oxide demonstrated very good accuracy of the Dyer model [9].

Waxman et al. have performed an extensive study on the two-phase flow of the nitrous oxide in the injectors [7]. They have identified two flow regimes that depend on the  $\Delta P$  and  $P_1$ . For low  $\Delta P$ , the mass flow rate can be estimated by the SPI model, while for given  $\Delta P$  the transition to the critical flow occurs, after which the two-phase models must be used. Waxman et al. compared experimental data with the critical flow predicted by the Dyer model with the majority of the values within  $\pm 10\%$ , but have not compared the data to the HEM model [7].

However, they have performed experiments with externally pressurized nitrous oxide above its saturation pressure, while most of the rockets using nitrous oxide work in self-pressurization mode. In external pressurization, inert gas such as nitrogen or helium from the separate tank keeps the pressure inside the nitrous oxide tank and feed system above its saturation pressure. Usually, the pressure can be controlled, allowing for adjustment of the propellant flow out of the tank. By keeping the pressure above saturation pressure of the nitrous oxide, the liquid does not boil in the tank and feed system. Thus no vapor is formed. However, this solution adds complexity to the system, as it requires an additional high-pressure tank and instrumentation to be installed in the rocket.

No additional gas is used in self-pressurizing mode, as the propellant is pushed out of the tank by its vapor pressure. Therefore, no extra components are needed, and the rocket system is greatly simplified. However, the propellant flow out of the tank causes the static pressure to drop below the saturation pressure of the nitrous oxide. The liquid in the tank and feed system boils, and vapor is formed, which leads to the two-phase flow in the entire system.

Self-pressurization is widely used for hybrid rockets due to its simplicity. Still, there is little data available on the impact of self-pressurization on the two-phase flow of the propellant. As, in the self-pressurizing mode, the vapor is formed not only in the injector but also in the feed system and the tank, the fluid reaches upstream of the injector with  $QF > 0$ , which presumably has a substantial effect on the flow behavior in the injector.

The purpose of this work is to provide better insight into the two-phase flow of the self-pressurizing propellants in the injector. It is underlined that the key intention is to study the system as it is used in the self-pressurizing rockets, which includes the feed system. The goal is to identify the flow regimes and validate the applicability of the SPI and HEM models in their respective regions. Additionally, an emphasis is put on studying the effect of the  $L/D$  on the flow, as it is a useful injector design parameter.

## 2. Experimental Setup

### 2.1. Test Stand

A dedicated test stand has been developed to characterize the mass flow rate of self-pressurizing nitrous oxide, enabling the simulation of the operating conditions in the rocket engine. The goal of the test stand is to study two-phase flow as it occurs in actual self-pressurizing rockets and not only isolate the effects of two-phase flow in the injector. The self-pressurization effects, such as boiling in the tank and feed system, need to be considered. Therefore, the test stand is designed similarly to the feed system in self-pressurizing hybrid rockets.

The photo of the test stand is shown in Figure 1. The key apparatus components are the run tank (3), the main valve (5), the chamber (7), and the injector (6). The tank is suspended on the load cell (1) that allows measurement of the instantaneous mass of the propellant in the tank (3). The tank is connected to the main valve and chamber assembly by the U-shaped flexible tube (9). When the main valve is open, the nitrous oxide flows from the tank through the injector into the chamber, where it expands. The run tank has a length of 220 mm and an internal diameter of 40 mm. The total volume of the run tank is approximately 0.28 L. The chamber has a length of 400 mm and an internal diameter of 40 mm. The inner diameter of the tubes is 4 mm. The load cell's full-scale accuracy is approximately  $\pm 5$  g.

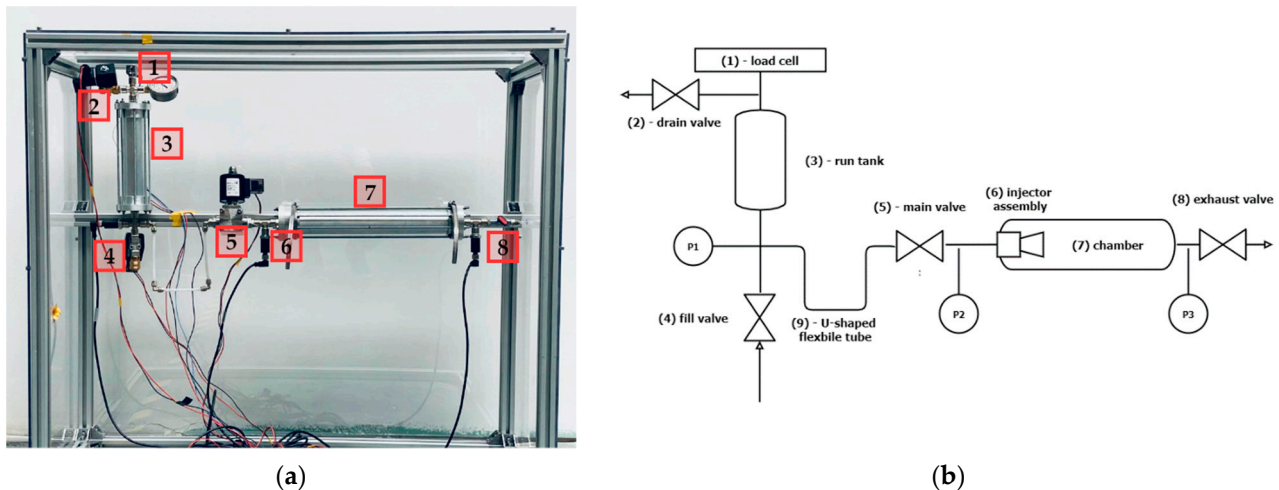


**Figure 1.** (a) Photo of the test stand, (b) Schematic diagram of the test stand. 1—load cell, 2—drain valve, 3—run tank, 4—fill valve, 5—main valve, 6—injector assembly, 7—chamber, 8—exhaust valve, and 9—U-shaped flexible tube. The storage tank and fill tube are not shown.

The flexible fill tube connects the run tank to the external storage tank (not shown in Figure 1). The fill (4) and drain valves (2), installed on the top and bottom of the run tank, are used to control the filling process. The test procedure and filling process are described later.

The injector assembly is mounted on the chamber and separates the downstream and the upstream. It contains replaceable orifice inserts that allow to easily test various injector designs. The schematic of the chamber with the injector assembly is shown in Figure 2a. Injector inserts are made of brass and sealed with an O-ring (Figure 2b).

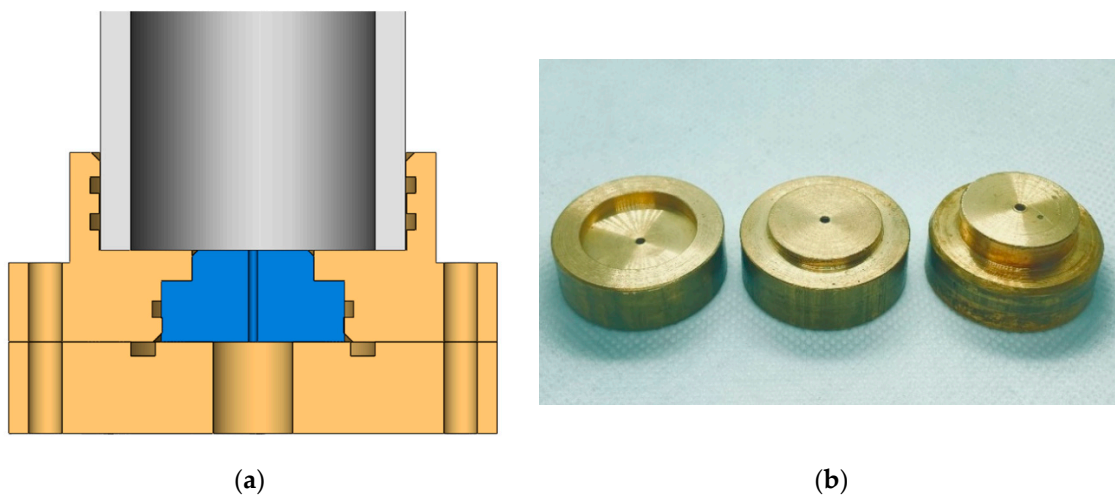


**Figure 2.** (a) CAD cut-away of the injector assembly on the chamber: injector assembly (orange), injector orifice (blue), and chamber (grey) (b) Photo of the Injector No. 1, No. 2, and No. 3.

A series of injectors with a different geometry is used in this study to characterize the mass flow rate with different length-to-diameter ratios ( $L/D$ ). Each injector has a simple, straight orifice with the sharp edge of the same diameter (1.5 mm) but varies in length. For the purpose of this study, five injector designs have been prepared with geometries given in Table 1. The increase in length for consecutive injectors is added on the downstream chamber side so that each injector has the same inlet geometry.

The pressures are measured in the tank, upstream of the injector (after the valve), and in the downstream chamber. From that, the instantaneous vapor pressure and pressure drop on the injector can be determined.

**Table 1.** The geometry of the injector orifices used in the study.

Injector No.	D (mm)	L (mm)	L/D
1	1.5	4.0	2.7
2	1.5	7.0	4.7
3	1.5	12.0	8.0
4	1.5	18.0	12.0
5	1.5	30.0	20.0

The instantaneous mass flow rate measurement is crucial to characterize the behavior of the two-phase flow of the propellant in the injector. However, conventional methods used to measure the mass flow rate cannot be readily used due to the two-phase flow of the nitrous oxide from the tank to the chamber. For example, venturi or mechanical flow meters require the density of the fluid to be known, which cannot be determined for the boiling nitrous oxide flow. Similarly, the Coriolis flow meter, which seems the best option to precisely measure the two-phase flow rate, would provide unreliable readings. The Coriolis meter depends on the vibration measurement of the internal flow tubes, which are designed to oscillate with a given frequency and amplitude. The two-phase may dampen the vibration, which leads to unreliable readings. This effect is severe when the vapor is high in the two-phase flow (high void fraction).

For this reason, the authors have decided to use an indirect measurement with the run tank suspended on the load cell, from which the data is differentiated to obtain the mass flow rate. However, this approach has several issues: (a) the run tank is mechanically connected to the chamber assembly and the storage tank by the flexible tubes, which corrupts the mass measurement, and (b) the numerical differentiation of the noisy measurement produces poor quality data. The authors have developed a series of workarounds to obtain reliable mass flow rate data shortly discussed below.

The mechanical connection from the run tank to the chamber obviously cannot be removed, while the fill tube from the storage tank cannot be unplugged once the run tank is filled for safety reasons. The flexible tubes degrade the mass measurement by their own weight and tension. While the weight can be accounted for with an offset, the tension results from the bending, pressure, and thermal stresses, significantly shifting during the test. The bent flexible tube works as a spring with given stiffness, which changes with the pressure inside. To remove these adverse effects, the bending of the tubes has been avoided, and room for tension compensation has been made. The U-shaped connection using three straight tubes has been used between the run tank and the chamber, while a sufficiently long tube has been installed to the storage tank and fixed at the neutral position perpendicularly to the run tank axis.

The mass measurements have been taken at the high frequency from 200 Hz up to 1 kHz and initially filtered with the Butterworth low-pass filter. Then, the Savitzky–Golay filter is applied with differentiation and proper window length. This approach reduces the number of data points significantly, but ensures the useful quality of the mass flow rate. The single flow test duration is of the order of ten seconds, and changes in the pressure and mass flow rate are several orders slower than the sampling intervals. Filtering of the data reduces measurement noise, which is necessary to obtain instantaneous values of the mass flow rate.

The implemented countermeasures have rendered the dynamic mass flow rate acquisition using the load cell feasible. The tests with water as a working fluid have been performed to verify if the mass flow rate measurement method is valid. Water tests have been performed for the different pressure conditions with well-characterized injector orifices. Instantaneous values of the mass flow rate have been compared with the Coriolis mass flow meter (Figure 3). The measured mass flow rate is within  $\pm 10\%$  of that given by the flowmeter. As the method relies on the changing total weight of the tank, the fluid phase shall have no impact on the readings. Then, the setup has been tested with nitrous oxide using different operating conditions such as pressures, temperatures, and fluid mass

in the tank to verify if the obtained mass flow rate data is reliable. The initial fluid mass in the tank has been compared to the value of the integrated mass flow rate obtained by the method. The adverse effects of the mechanical coupling and the differentiation have been significantly reduced to the level enabling the characterization of the two-phase mass flow rate. The residual impact of the mechanical coupling is examined later in the paper.

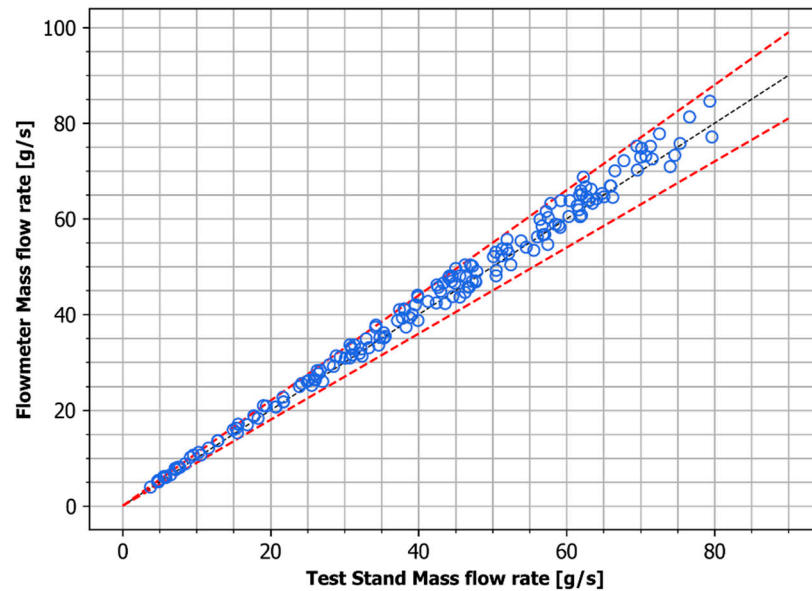


**Figure 3.** Comparison of the mass flow rate measured using the test stand to that measured using the Coriolis flowmeter. The measured mass flow rate is within  $\pm 10\%$  of the actual (given by the flowmeter).

## 2.2. Test Procedure and Data Analysis

Before the test, the run tank is filled with liquid nitrous oxide from the storage tank, as described earlier. Initially, the run tank is empty, and the solenoid fill valve at the bottom of the tank is opened. The initial surge of the fluid can fill the tank with liquid to some level, but the nitrous oxide quickly pressurizes the tank to its vapor pressure. As only self-pressurization is used for the filling process, the pressure in the run tank and storage tank reaches the same level, and the liquid stops flowing. Usually, at this point, the run tank is only partially filled with liquid. The drain valve at the top of the run tank is used to force more liquid into the run tank. It is opened for a short time to release some vapor and provide a pressure difference between the run tank and storage tank, which drives liquid from the storage tank. This way, the run tank can be filled with liquid to the desired level.

After the run tank is filled, the test can be initiated by opening the main valve. It is a fast-acting, high-flow solenoid valve to ensure low-pressure drop and quick pressure build-up upstream of the injector. Nitrous oxide immediately starts to flow from the run tank to the chamber (Figure 4 at 0 s). The tank pressure  $P_t$  drops rapidly, but levels out as soon nitrous oxide fills the upstream injector volume (45 bar at 0.3 s). The upstream pressure  $P_1$  settles, and the flow through the injector is established (0.5 s). Chamber pressure  $P_2$  rises as nitrous oxide enters through the injector orifice and expands. The chamber is usually vented during the test with a very small exhaust orifice (1–1.5 mm) to ensure the desired rate of pressure build-up. Chamber pressure  $P_2$  takes few seconds to rise, during which the upstream pressure  $P_1$  is roughly at the same level. This enables us to measure mass flow rate in a wide range of injector pressure drop  $\Delta P$ . As the nitrous oxide operates in self-pressurizing mode, and there is a significant pressure drop in the feed system ( $P_t - P_1$ ), a large amount of vapor is formed, and fluid reaches the upstream injector volume in a two-phase state. During the test, the nitrous oxide boils in the run tank, which lowers its bulk temperature and vapor pressure, which is reflected in decreasing  $P_t$  and  $P_1$  (liquid boils from 0 s up to its depletion at approx. 4 s). Typical test pressure history is given in Figure 4.

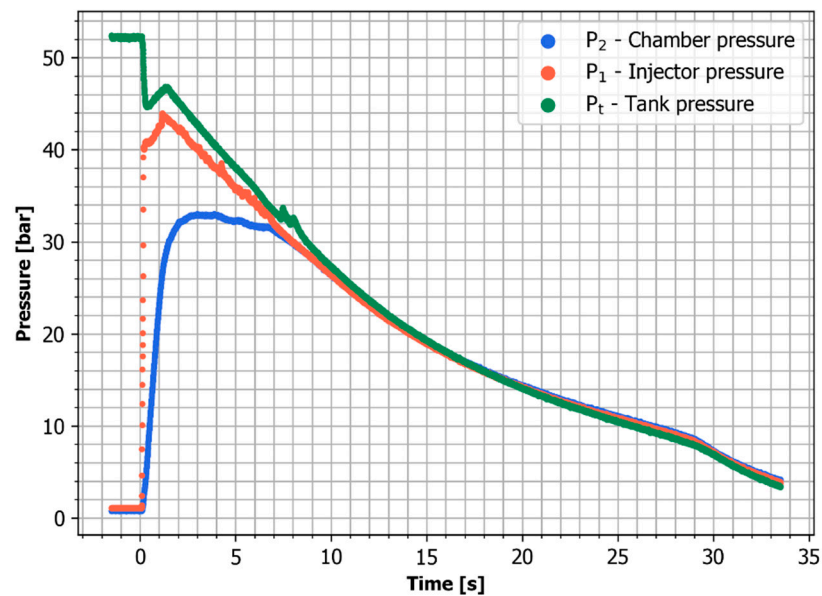


**Figure 4.** Pressure time history of a typical test. The valve opens at approximately 0 s. Data for the Injector No. 2.

The test concludes after all nitrous oxide vents through the chamber exhaust orifice. However, much sooner, all the liquid in the system is depleted. This fact is mainly detected by the transition in mass flow rate, which is depicted in Figure 7. During the test, the mass flow rate follows a roughly linear path, while there is a sudden drop at the liquid depletion. The point at which the liquid has been depleted cannot be precisely determined, so the transition is chosen based on the deviation from the linear path. Such an approach is supported by the experimental results from other works on self-pressurizing rockets by the authors [11,12]. Usually, in the self-pressurizing rocket engines, the liquid depletion can be easily detected by the transition in the vapor pressure, but in this setup, the pressure transition is hardly noticeable due to the relatively large amount of vapor in the system and low exhaust flow rate. For this work, only the region with the liquid present is of importance. Figure 5 shows the typical mass measurement history during the test.

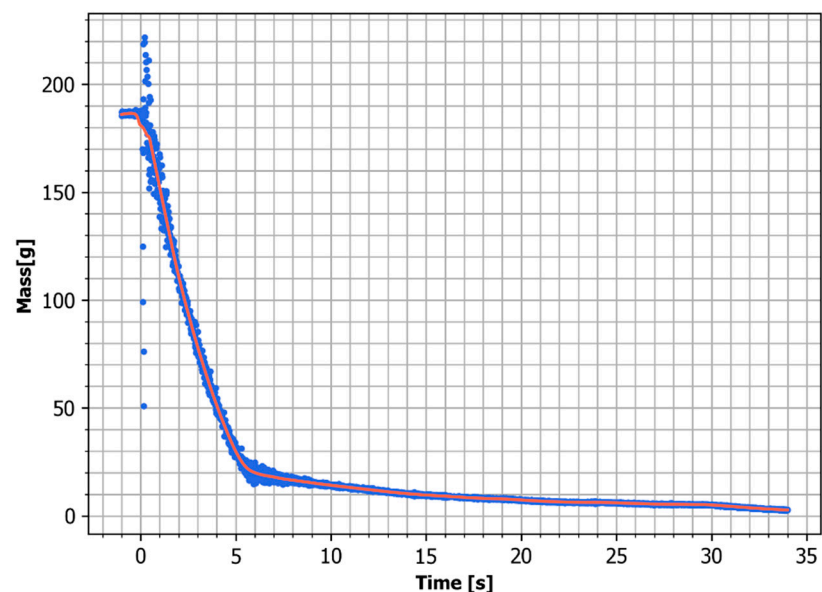


**Figure 5.** Run tank mass time history of a typical test. The valve opens at approximately 0 s. Scattered data can be seen during the initial phase. Data for the Injector No. 2.

When the main valve opens, several factors contribute to the initial scatter of the signal: (a) fast main valve opening introduces some vibration, which is transferred to the suspended run tank by the feed system, (b) initial surge of the fluid from the run tank to the upstream of the injector, during which the mass flow rate is very high, and (c) the vibration induced by the momentum of the initial surge. As soon as the upstream injector volume is filled and  $P_1$  levels out, the mass flow rate stabilizes, and the vibration on the load cell dampens. For the reasons mentioned above, the data for the analysis must be correctly trimmed, as shown in Figure 6 by yellow region, to include only relevant data. Typical data ready for analysis is depicted in Figure 7. A detailed description of the results and discussion on the mass flow characteristics are presented in the following sections.

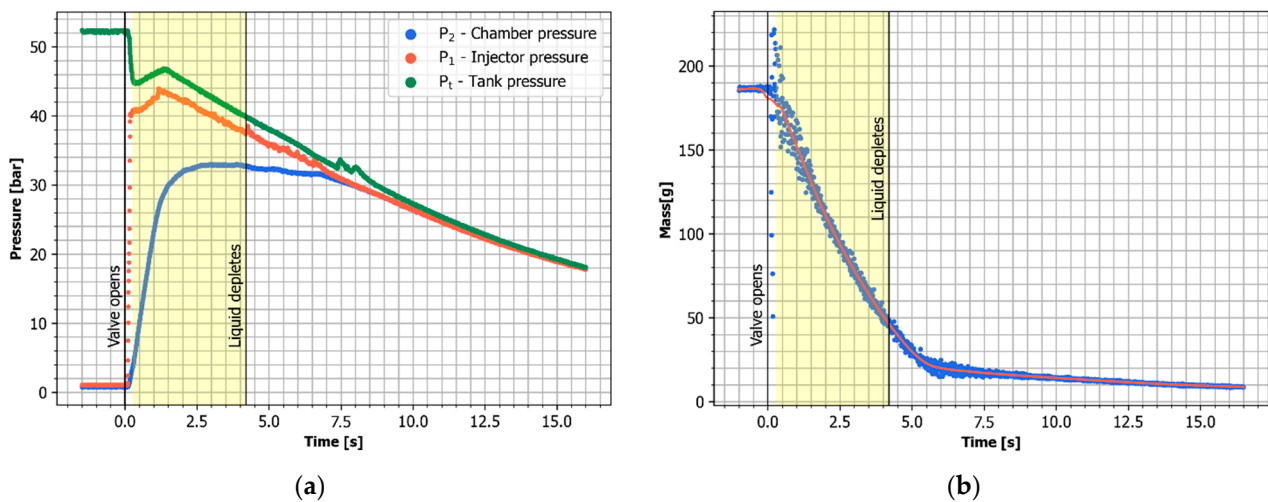


**Figure 6.** Data trimming for a typical test: (a) pressure time history, (b) run tank mass time history. Data for the Injector No. 2.

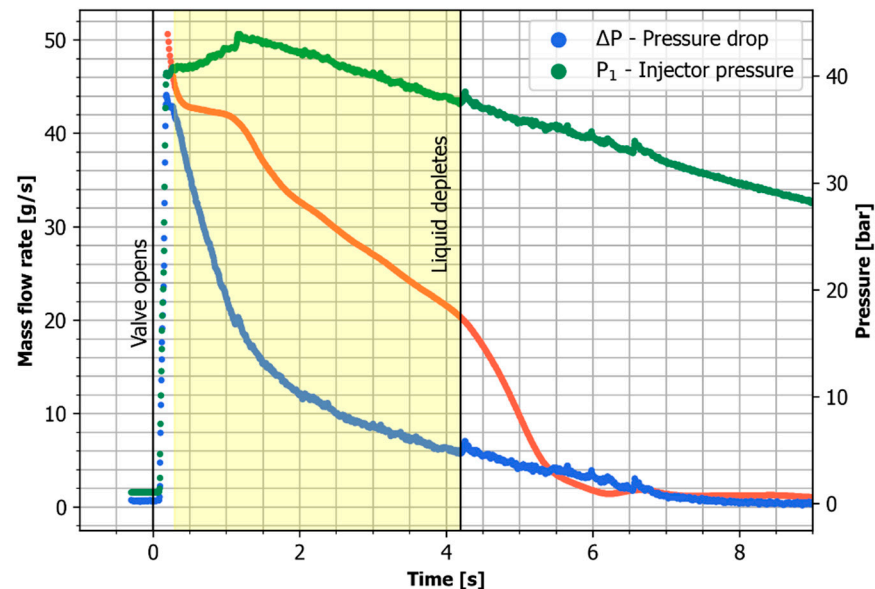


**Figure 7.** Injector pressure drop  $\Delta P$  and vapor pressure  $P_1$  plotted with mass flow rate (red) calculated from the mass measurement. Liquid depletion is identified by the sudden drop of the mass flow rate. The yellow region shows relevant data trimming for the analysis. Data for the Injector No. 2.

### 3. Results

Tests have been performed for every injector design given in Table 1 for the same initial operating conditions. Initial temperature and vapor pressure of the saturated nitrous

oxide in the storage tank and the run tank have been kept at roughly  $P_v = 52$  bar and  $T_1 = 294.4$  K. The typical initial mass of the nitrous oxide filled in the run tank was 180–190 g. This gives ullage volume of about 15%. The following sections describe the results of the experiments, including the identification of the flow regimes and the effect of the L/D ratio.

### 3.1. Flow Regimes

It is necessary to plot the mass flow rate versus pressure drop to examine mass flow characteristics, as shown in Figure 8. It must be noted that due to the self-pressurization, the vapor pressure  $P_1$  decreases during the test, which additionally impacts the mass flow rate but cannot be easily accounted for in Figure 8.

However, to analyze the behavior of the flow, the predicted mass flow rate by the SPI and HEM models are plotted on the experimental data, using Equations (1) and (4), respectively. The values from SPI and HEM have been calculated using instantaneous pressure data from the test, which includes both  $\Delta P$  and  $P_v$ . This way, Figure 8 can be used to examine the mass flow rate behavior with operating conditions in the rocket engine with self-pressurization.

In Figure 8, depicting the data for the Injector No. 2, two flow regimes can be clearly identified: for approximately  $\Delta P < 17.4$  bar, the flow follows the SPI model predictions, while for larger values of  $\Delta P$  the critical flow occurs, which is finely predicted by the HEM model. The discharge coefficient used to fit the SPI, and HEM models have been chosen such that: (a) for HEM, the  $C_d^{\text{water}}$  has been assumed from the water tests on the injector, and (b) for SPI, the  $C_d^{\text{SPI}}$  has been tailored to fit the curve into data points. It must be noted that the nitrous oxide in the upstream and injector orifice is in a two-phase state; therefore, SPI model is physically not valid. Similarly, the HEM model assumes that the nitrous oxide is saturated liquid in the upstream, which is also not true. Still, it seems that the flow can be described by those models in these two flow regimes. Further discussion on the potential explanation is given in the later section.

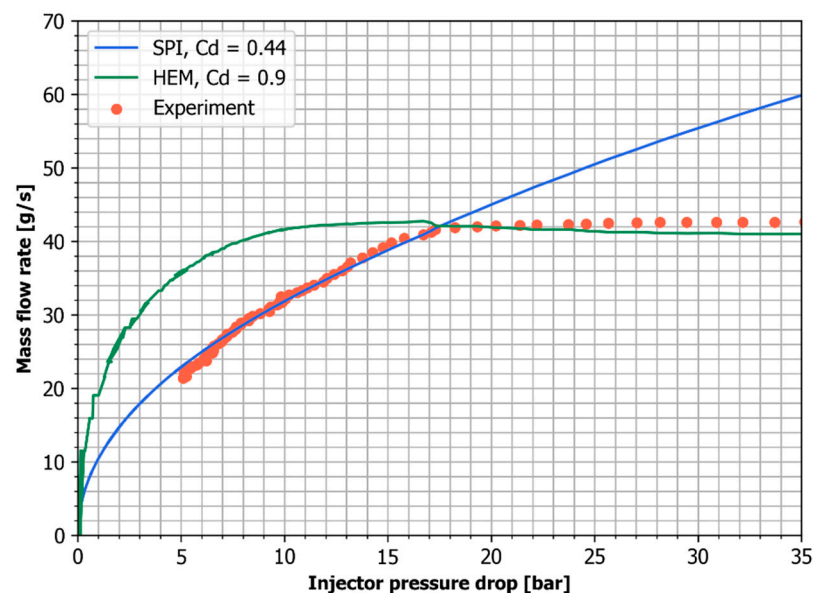


**Figure 8.** Mass flow rate versus injector pressure drop  $\Delta P$  for the Injector No. 2. SPI and HEM curves have been plotted using pressure data from the test.

### 3.2. Effect of the L/D on the Critical Flow

For each injector, the critical flow has occurred at different injector pressure drop  $\Delta P$ . Figure 9 provides mass flow rate data for all injectors plotted versus  $\Delta P$ , but for convenience, the critical flow data are gathered in Table 2. To account for different vapor pressure  $P_1$  in each test, it is useful to plot mass flow rate versus the ratio of chamber

pressure  $P_2$  and vapor pressure  $P_1$  as depicted in Figure 10. As described earlier, it is thought that the mass flow rate is independent of the downstream chamber pressure conditions in the critical flow region. In fact, for each injector, there is a given  $P_2/P_1$  ratio below which the mass flow rate is roughly at a constant level. The critical flow transition is plotted versus the L/D ratio in Figure 11.

**Table 2.** Critical flow data for all injectors.

Injector No.	L/D	Critical $\Delta P$ (bar)	Critical $\dot{m}$ (Average) (g/s)
1	2.7	$17.0 \pm 0.9$	$45.4 \pm 5.0$
2	4.7	$17.4 \pm 0.9$	$42.5 \pm 5.0$
3	8.0	$14.5 \pm 0.7$	$42.0 \pm 5.0$
4	12.0	$13.6 \pm 0.7$	$41.6 \pm 5.0$
5	20.0	$10.6 \pm 0.5$	$40.3 \pm 5.0$

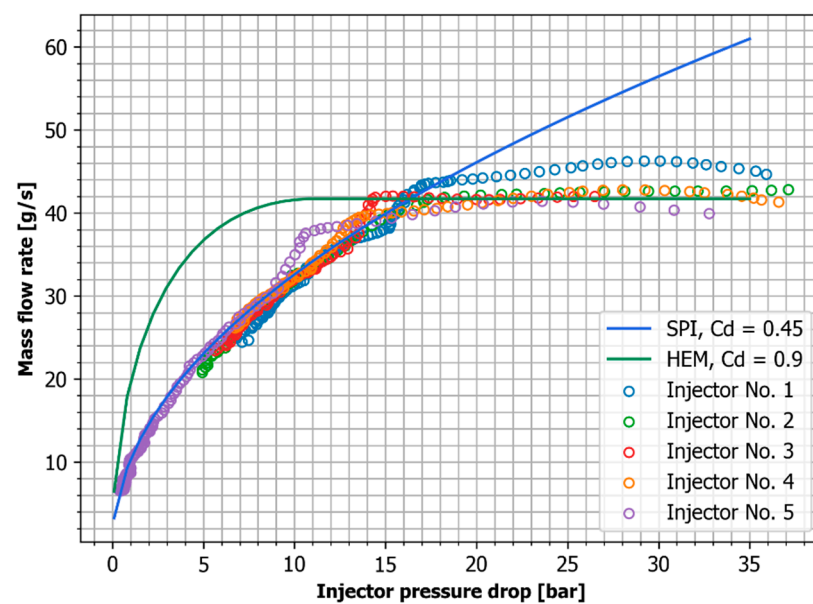


**Figure 9.** Mass flow rate versus injector pressure drop  $\Delta P$  for all injector designs. SPI and HEM curves are roughly fitted, showing similar flow performance for the injectors.

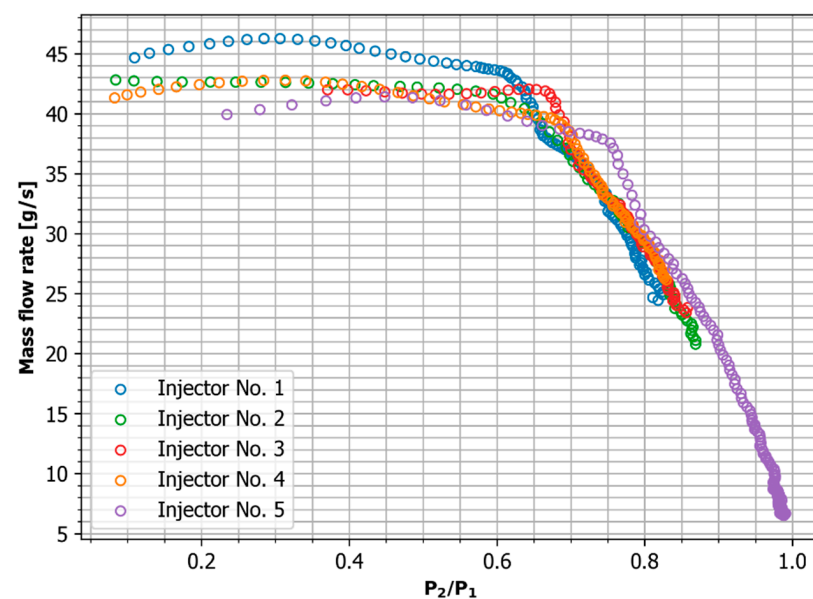


**Figure 10.** Mass flow rate versus the ratio of chamber pressure and upstream pressure for all injectors.

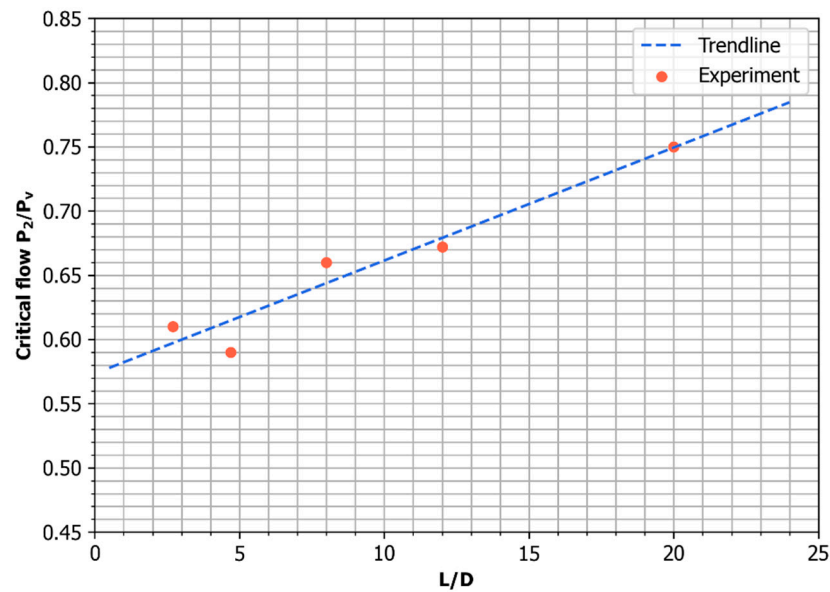


Figure 11. Effect of the L/D ratio on the critical flow transition.

## 4. Discussion

### 4.1. SPI Flow Regime

The following section discusses gathered results focusing on the flow regimes and the effect of the self-pressurization on the mass flow rate prediction using SPI and HEM models and the impact of the L/D on the two-phase flow.

Figure 9 shows that the flow curves for injectors with different L/D and the same initial operating conditions are similar in the sense that all: (a) follow the SPI model up to the critical flow transition, and (b) exhibit critical flow past given  $\Delta P$ , which the HEM model predicts. This behavior is consistent with previous findings [7].

However, there is a significant discrepancy when it comes to the value of the discharge coefficient  $C_d$ . In the study performed by Waxman et al., the  $C_d$  in the SPI region ( $C_d^{SPI}$ ) is constant and equal to the discharge coefficient of the single-phase fluid. In this work, the  $C_d^{SPI}$  is significantly lower than the  $C_d^{water}$  measured for the single-phase fluid (water). For every injector design, the measured  $C_d^{water}$  is approximately 0.9, while the  $C_d^{SPI}$  is roughly 0.45. We reason that it is due to the self-pressurization mode, which resulted in a high vapor amount upstream of the injector, consequently congesting the mass flow rate already in the SPI region. Waxman et al. have studied the nitrous oxide with external pressurization above the vapor pressure of the nitrous oxide (called supercharge), which resulted in no vapor upstream of the injector ( $QF = 0$ ). The upstream QF cannot be easily measured or deduced from the gathered data in this study, but it is certainly non-zero.

To estimate the upstream QF, we have performed a short analysis. Assuming that in the SPI region, the vapor and liquid are in equilibrium and the velocity of the phases is the same (flow without slip,  $S = 1$ ), the mass flow rate can be expressed by:

$$\dot{m}_t = \dot{m}_v + \dot{m}_l, \quad (5)$$

where the vapor and liquid mass flow rates are given by the SPI model, including the void fraction  $\alpha$ :

$$\dot{m}_v = \alpha C_d A \sqrt{2\rho_v \Delta P}, \quad \dot{m}_l = (1 - \alpha) C_d A \sqrt{2\rho_l \Delta P} \quad (6)$$

Then, by substituting measured mass flow rate for  $\dot{m}_t$  and assuming  $C_d = C_d^{water}$ , the  $\alpha$  can be calculated by:

$$\alpha = \frac{\dot{m}_t - \dot{m}_l}{\dot{m}_v - \dot{m}_l} \quad (7)$$

and from that, the QF is obtained:

$$QF = \frac{1}{1 + \frac{1-\alpha}{\alpha} \frac{\rho_l}{\rho_v}} \quad (8)$$

Using the above method, we have calculated the QF in the SPI region, which equals 0.39–0.50 for the tested injectors. It may seem that the presence of the vapor upstream of the injector ( $QF > 0$ ) effectively reduces the  $C_d^{SPI}$  correspondingly to the flow quality. The reason for this is that as the SPI includes only a single phase, it does not account for the presence of the vapor in the flow, the density of which is much lower than the liquid. If we increase the vapor fraction in the flow (larger QF), then the effective bulk density will be lower. The difference between the measured mass flow rate and SPI values for non-zero QF comes from the lowered bulk density. This discrepancy is included in the discharge coefficient. This way, the  $C_d^{SPI}$  is reduced from its basic level measured for the single-phase liquid value. It must be kept in mind that the discharge coefficient also includes other effects, which reduces the measured value from the theoretical.

However, it cannot be assumed that there is no slip between the phases in the injector orifice, and as it has a significant effect on the two-phase mass flow rate, the above logic cannot be readily used to conclude the effect of the estimated QF on the effective discharge coefficient  $C_d^{SPI}$ . If the upstream QF is majorly affecting the discharge coefficient in the SPI region, then it is an important design factor that needs to be accounted for. The QF seemingly depends on the feed system design that governs, e.g., the pressure drop and vapor promoting nucleation zones. The impact of the upstream QF on the  $C_d$  and the means it can be included in the engineering design process of the injector and feed system in the nitrous oxide self-pressurized rockets will be studied in the future.

#### 4.2. Critical Flow Regime

In this study, the HEM model predicts the critical flow value reasonably well. The HEM curves have been found using pressure data from the test and the discharge coefficient measured for water ( $C_d^{water}$ ). A typical resultant HEM curve is given for injector No. 2 in Figure 8. For each injector the HEM model's predicted critical mass flow rate was in  $\pm 12.5\%$  error margin. We must note that such error margin results mostly from the measurement method uncertainties. The HEM model reportedly has significantly underpredicted the critical mass flow rate when the nitrous oxide has been studied with the supercharging [7] or self-pressurization [6], but also when analogous carbon dioxide has been used with self-pressurization [8]. We believe that the discrepancy between reported results is due to the impact of the feed system design on the flow. Similarly to the mechanism governing the two-phase flow in the injector, if the residence time and pressure drop in the feed system are high enough, the flow reaches the upstream of the injector with non-zero QF, which then affects the flow through the injector. The impact of the feed system on the flow and accuracy of the HEM model depends on the experimental setup that is used to study the flow in the injector.

Waxman et al. have used supercharged pre-injector volume, in which the nitrous oxide has been kept above saturation pressure. From that volume, the saturated nitrous oxide flows through the injector orifice. There is no boiling in the feed system (pre-injector volume), so flow reaches the injector with  $QF = 0$  [7]. Stannard et al. have used a similar setup but without supercharging. However, they have used large flow lines between the run tank and pre-injector volume, which resulted in minimal pressure drop in the feed system [8]. For their experiments, Whitmore et al. have used a modified commercially available hybrid rocket motor, in which the injector is the end cap of the oxidizer tank. As the tests were performed using self-pressurization and nitrous oxide is boiling in the tank, there is non-zero QF upstream of the injector (in the tank). However, there is no feed system between the tank and the injector, so there is no effect of the residence time and pressure drop in the feed system on the flow QF [9]. Dyer et al. have not disclosed the details of the experimental setup [6].

In this study, the feed system comprises roughly 30 cm of 4 mm tubes (bending 90° four times), 10 cm of 6 mm lines, and a high-flow (15 mm) valve. A mass flow rate of 30–40 g/s results in an average pressure drop of 4–5 bar from the tank to the injector. Due to that, the boiling in the feed system is significant, and when the flow reaches the upstream of the injector, it has a relatively high QF. In other studies, this effect has been eliminated or minimized so that upstream QF is either negligibly low or equals 0. For example, Stannard et al. reported a pressure drop from the run tank to the pre-injector volume of about 1.6 bar with mass flow rates over 1 kg/s.

We believe that the non-zero upstream QF due to the self-pressurization may increase the accuracy of the HEM model, as it supports the reaching of the equilibrium between the phases in the injector orifice, which is assumed in the HEM model. Paccagnella et al. have analyzed the injector data for a 1 kN hybrid rocket for the purpose of CFD simulation. They have included the effect of the feed system in the form of isenthalpic expansion and compared SPI and HEM models. The HEM underpredicted the flow by about 25%, while the SPI model has predicted the flow very well. However, the mass flow rate data they have compared has been extrapolated from the injector with very low  $L/D = 2$ . On the other hand, when using the HEM model to find the mass flow rate directly from the tank to the chamber ( $\Delta P = 30$  bar), without the isenthalpic expansion, they have obtained overprediction by only 3.5% [13]. Such an approach to include the feed system effect is interesting, but more systematic study is required.

It seems that the feed system design and upstream QF are important factors in the two-phase flow modeling through the injector, but more work needs to be completed on that subject.

Still, the HEM model fails to predict the transition to the critical flow in terms of  $P_2/P_1$ , which seems to depend on the  $L/D$  ratio, as shown in Figure 11. For low  $L/D$ , the critical flow starts when the chamber pressure drops below roughly 60% of the upstream pressure, while for very high  $L/D$ , the critical flow starts below 75% of the upstream pressure. It is related to the residence time in the orifice and pressure drop. The greater  $L/D$  increases the residence time in the orifice, so the flow has more time to reach thermal equilibrium (vaporize). The higher the residence time and pressure drop, the more the two-phase flow develops, at some point “choking” the orifice so that mass flow reaches its maximum (critical flow). As the larger  $L/D$  increases residence time, the orifices with high  $L/D$  reach the critical flow for smaller pressure drop, or in other words, for larger  $P_2/P_1$ . This is consistent with the previous findings [6,14].

The suggested effect of the  $L/D$  on the critical flow and the fact that the mass flow rate is independent of the chamber pressure in the critical flow regime can be used to design a rocket injector that promotes stable combustion and suppresses feed-coupled instabilities. It must be noted that, in this study, we have not varied the diameter of the orifice, only the length. Therefore, we cannot conclude on the effect of the  $L/D$  solely from our study, but the literature supports a similar effect of the  $L/D$  [6,10].

## 5. Conclusions

The flow of the self-pressurizing nitrous oxide in the injector has been studied on the dedicated test stand. The results confirm two flow regimes: the “single-phase region”, which follows the SPI curve, and the critical flow, which the HEM model predicts. The transition to the critical flow depends on the  $\Delta P$  and the  $L/D$  ratio of the injector’s orifice. The greater the  $L/D$ , the greater the  $P_2/P_1$  ratio for which the transition occurs. This information can be used to design hybrid rockets more immune to combustion instabilities.

When it comes to the prediction of the mass flow rate in the SPI regime, the  $C_d$  seems to depend on the upstream QF of the propellant. By adjusting the  $C_d$ , the flow in this regime is finely predicted by the SPI model. In this study, the HEM model predicted the mass flow rate in the critical flow region reasonably well, but failed to predict the transition point, which depends on other factors such as the  $L/D$  ratio. It is suggested that the

accuracy of the HEM model, when it comes to the critical flow value, depends on the QF upstream of the injector.

**Author Contributions:** Conceptualization, T.P. and J.C.; methodology, T.P.; software, T.P.; formal analysis, T.P.; investigation, T.P.; resources, T.P.; writing—original draft preparation, T.P.; writing—review and editing, T.P. and J.C.; visualization, T.P.; supervision, J.C.; project administration, J.C.; and funding acquisition, J.C. All authors have read and agreed to the published version of the manuscript.

**Funding:** This research was funded by the AGH University of Science and Technology.

**Data Availability Statement:** The data presented in this study are available on request from the corresponding author.

**Conflicts of Interest:** The authors declare no conflict of interest.

## References

1. Nosseir, A.E.S.; Cervone, A.; Pasini, A. Review of State-of-the-Art Green Monopropellants: For Propulsion Systems Analysts and Designers. *Aerospace* **2021**, *8*, 20. [[CrossRef](#)]
2. Kobald, M.; Fischer, U.; Tomilin, K.; Petrarolo, A.; Schmierer, C. Hybrid Experimental Rocket Stuttgart: A Low-Cost Technology Demonstrator. *J. Spacecr. Rocket.* **2018**, *55*, 484–500. [[CrossRef](#)]
3. Dyer, J.; Doran, E.; Dunn, Z.; Lohner, K.; Bayart, C.; Sadhwani, A.; Zilliac, G.; Cantwel, B.; Karabeyoglu, A. Design and Development of a 100 km Nitrous Oxide/Paraffin Hybrid Rocket Vehicle. In Proceedings of the 43rd AIAA/ASME/SAE/ASEE Joint Propulsion Conference & Exhibit, Cincinnati, OH, USA, 8–11 July 2007; Volume 4, pp. 3550–3558. [[CrossRef](#)]
4. Zakirov, V.; Sweeting, M.; Lawrence, T.; Sellers, J. Nitrous oxide as a rocket propellant. *Acta Astronaut.* **2001**, *48*, 353–362. [[CrossRef](#)]
5. Hesson, J.C.; Peck, R.E. Flow of two-phase carbon dioxide through orifices. *AIChE J.* **1958**, *4*, 207–210. [[CrossRef](#)]
6. Dyer, J.; Zilliac, G.; Sadhwani, A.; Karabeyoglu, A.; Cantwell, B. Modeling Feed System Flow Physics for Self-Pressurizing Propellants. In Proceedings of the 43rd AIAA/ASME/SAE/ASEE Joint Propulsion Conference & Exhibit, Cincinnati, OH, USA, 8–11 July 2007; Volume 7, pp. 6835–6847. [[CrossRef](#)]
7. Waxman, B.S.; Cantwell, B.; Zilliac, G.; Zimmerman, J.E. Mass Flow Rate and Isolation Characteristics of Injectors for Use with Self-Pressurizing Oxidizers in Hybrid Rockets. In Proceedings of the 49th AIAA/ASME/SAE/ASEE Joint Propulsion Conference, San Jose, CA, USA, 14–17 July 2013; Volume 1, pp. 1–32. [[CrossRef](#)]
8. Stannard, D.; Quinn, D.; Hill, C.; Johansen, C. Experimental investigation of self-pressurized propellant injection into a simulated rocket motor combustion chamber. *Int. J. Multiph. Flow* **2021**, *142*, 103707. [[CrossRef](#)]
9. Whitmore, S.; Chandler, S.N. Engineering Model for Self-Pressurizing Saturated-N<sub>2</sub>O-Propellant Feed Systems. *J. Propuls. Power* **2010**, *26*, 706–714. [[CrossRef](#)]
10. Darby, R.; Meiller, P.R.; Stockton, J.R. Select the best model for two-phase relief sizing. *Chem. Eng. Prog.* **2001**, *97*, 56–64.
11. Palacz, T. Nitrous Oxide Application for Low-Thrust and Low-Cost Liquid Rocket Engine. In Proceedings of the 7th EUCASS, Milano, Italy, 3–7 July 2017. [[CrossRef](#)]
12. Palacz, T.; Postulka, B.; Dro, P. Design and Development of a Nitrous Oxide/Alcohol Sounding Rocket Technology Demonstrator. In Proceedings of the 8th EUCASS, Madrid, Spain, 1–4 July 2019. [[CrossRef](#)]
13. Paccagnella, E.; Barato, F.; Gelain, R.; Pavarin, D. CFD Simulations of Self-pressurized Nitrous Oxide Hybrid Rocket Motors. In Proceedings of the Joint Propulsion Conference, Cincinnati, OH, USA, 9–11 July 2018. [[CrossRef](#)]
14. Henry, R.E.; Fauske, H.K. The Two-Phase Critical Flow of One-Component Mixtures in Nozzles, Orifices, and Short Tubes. *J. Heat Transf.* **1971**, *93*, 179–187. [[CrossRef](#)]